

Direct Synthesis of Far-Field Patterns

Gaobiao Xiao ¹

¹Shanghai Jiao Tong University

December 13, 2023

Abstract

I feel sorry that the manuscript is written in a hurry and most content of the synthesis of the linear arrays is similar to that discussed in C.A. Balanis book as pointed out by reviewers. However, I still post this manuscript on this server as I indeed derived it from the very beginning and I wish some part of them may be of usage for others, especially the 2-D cases and some of my considerations on this issue. The direct synthesis results are very good initial values for further optimization with a method in which the properties of the entire functions and the number of degrees of the freedom of far fields are made full use of.

In this paper, the current distribution is expanded with Fourier series. Analysis shows that only a limited number of the harmonic components of the current can generate propagation fields and contribute to the far-field pattern. Most importantly, it is found that this part of the current can be directly obtained from the far-field without utilizing any optimization algorithm. The degree of freedom of the far-field can be exactly counted for a linear source or a rectangular planar source. Numerical examples verify that the method is very efficient for synthesizing large antenna arrays.

Direct Synthesis of Far-Field Patterns

Gaobiao Xiao, *Senior Member, IEEE*

Abstract—In this paper, the current distribution is expanded with Fourier series. Analysis shows that only a limited number of the harmonic components of the current can generate propagation fields and contribute to the far-field pattern. Most importantly, it is found that this part of the current can be directly obtained from the far-field without utilizing any optimization algorithm. The degree of freedom of the far-field can be exactly counted for a linear source or a rectangular planar source. Numerical examples verify that the method is very efficient for synthesizing large antenna arrays.

Index Terms—Radiation field, degree of freedom, antenna array synthesis

I. INTRODUCTION

LARGE antenna arrays are well used in massive MIMO systems [1][2], radio telescope [3], modern radar systems [4] and satellite communications [5]. In many applications, the arrays are composed of antenna elements positioning with spacing of half wavelength along a straight line, or on a plane or a conformal surface. The elements usually have identical radiation performance. The radiation pattern of the array is the product of the array factor and the element factor. Radiation pattern synthesis technique [6] may have to be used in some situations where it is required to control the footprint of satellite antennas to illuminate coverage area [8], or to reduce side lobe levels to avoid known interference spots [9][10], or to realize pencil beams[12] or multiple beams[13], and so on. However, most of the synthesis approaches are based on some kind of optimization strategy, e.g., genetic algorithms (GAs)[14][15], particle swarm optimization (PSO)[16], simulated annealing (SA) [17], sequential convex optimizations[18][19], and some other algorithms [20]-[29]. These optimization methods have also been successfully applied for synthesizing sparse arrays [30]. The Fast Fourier Transform (FFT) can be used to accelerate the optimization in some cases [10]. An analytical method to determine the positions of the elements of an unequally-spaced arrays was proposed in [31]. Unfortunately, all these methods are often time consuming, especially for very large-scale arrays.

It is not the purpose of this paper to review and compare all these conventional methods. In this paper, we revisit this synthesis issue from re-considering the radiation problem of a current source in vacuum. A linear current and a planar current on a rectangular sheet are examined. A key trick we adopted here is that the size of the source region is assumed to be multiple wavelengths in one dimension. The current sources are

expanded with Fourier series. Each harmonic component of the current source generates an electromagnetic field in the space, and is described with a sinc mode function. All field modes are divided into two groups based on their properties. One is the propagation group consisting of all propagation modes that can contribute to the far-field pattern. The other is the evanescent group consisting of all evanescent modes that decay exponentially away from their source and do not contribute to the far-field pattern. The far-field is then exactly expressed as a superposition of the propagation modes. Each propagation mode has a main beam, the peak of which is positioned in the visible region of the antenna array. Most importantly, by setting the restriction on the source sizes, the zero points of one propagation mode coincides with the zero points or the peak of the other propagation modes. Therefore, the far-field is expressed as an ideal interpolation using sinc mode functions, with values sampling at the peak of the propagation modes. Consequently, the Fourier coefficients of the current can be directly obtained with no necessary to solve any equation or utilizing any optimization algorithm. The current distribution is then readily calculated directly or using FFT.

This paper is organized as follows. The one-dimensional (1-D) case is discussed in Section II, where the properties of the propagation mode is discussed. The expressions for calculating the current source for realizing a prescribed far-field pattern is provided. The two-dimensional (2-D) case is discussed in Section III, and some related topics are discussed in IV. Numerical examples are provided in the corresponding sections.

II. THE ONE-DIMENSIONAL CASE

The electric field of a current $\mathbf{J}(\mathbf{r}')$, $\mathbf{r}' \in V_s$, at the position \mathbf{r} in far region can be generally expressed as

$$\mathbf{E}(\mathbf{r}) = (\bar{\mathbf{I}} - \hat{\mathbf{a}}_r \hat{\mathbf{a}}_r) \cdot \frac{e^{-jk_r r}}{4\pi r} \int_{V_s} e^{jk_r \mathbf{r}'} \mathbf{J}(\mathbf{r}') d\mathbf{r}' \quad (1)$$

where $\mathbf{k} = k_x \hat{\mathbf{a}}_x + k_y \hat{\mathbf{a}}_y + k_z \hat{\mathbf{a}}_z$ is the wave vector, $\hat{\mathbf{a}}_r$ is the radial unit vector, and $\bar{\mathbf{I}}$ is the identity operator. Consider a linear source $I(z) \hat{\mathbf{a}}_z$, $-D_z/2 \leq z \leq D_z/2$, as shown in Fig.1. Its far-field can be expressed as

$$\mathbf{F}(\theta) = -\hat{\mathbf{a}}_\theta \sin \theta \int_{-D_z/2}^{D_z/2} e^{jk_z z} I(z) dz \quad (2)$$

where $k_z = k \cos \theta$. We choose $D_z = N_z \lambda$, in which λ is the wavelength and N_z is an integer.

A linear current source can be considered as an array of the infinitesimal dipole with the element factor of $\sin \theta$, so the array factor of the linear current may be expressed as

$$F_a(\theta) = \frac{1}{D_z} \int_{-D_z/2}^{D_z/2} e^{jkz \cos \theta} I(z) dz \quad (3)$$

Here, a constant factor $(1/D_z)$ is used for the sake of convenience. In this paper, we focus on the synthesis of the array factor so that the results can be extended to arrays with other types of elements. The linear current can be expanded with 1-D Fourier series,

$$I(z) = \sum_{n=-\infty}^{\infty} I_n e^{jn\Omega z} \quad (4)$$

where $\Omega = 2\pi/D_z = k/N_z$, k is the wavenumber and $k = 2\pi/\lambda$.

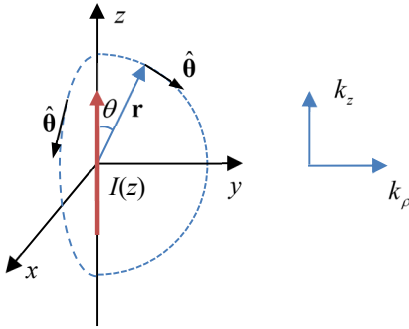


Fig.1 A linear current source on the z-axis.

Substituting (4) into (3) yields,

$$F_a(\theta) = \sum_{n=-\infty}^{\infty} I_n f_n(\theta) \quad (5)$$

In this paper, $f_n(\theta)$ is referred to as the n -th mode function. It is straight-forward to derive that

$$f_n(\theta) = \frac{\sin\left[\frac{(k_z + n\Omega)D_z}{2}\right]}{\frac{(k_z + n\Omega)D_z}{2}} = \text{sinc}\left[\frac{D_z}{2}(k \cos \theta - k_{zn})\right] \quad (6)$$

where $\text{sinc}(x) = \sin x/x$ and $k_{zn} = -n\Omega$. The mode function $f_n(\theta)$ reaches its peak value at $\theta = \theta_n$, and θ_n is determined by

$$\theta_n = \cos^{-1}(-n/N_z) \quad (7)$$

Each mode function $f_n(\theta)$ represents a beam that is axially symmetrical with respect to the linear source. The n -th beam, hereafter also referred to as the n -th mode, is located in the visible region if its peak direction satisfies $-\pi \leq \theta_n \leq \pi$, which leads to $-N_z \leq n \leq N_z$.

On the other hand, the transversal wavenumber k_p can be expressed as

$$k_p = \sqrt{k^2 - k_z^2} = k\sqrt{1 - (n/N_z)^2}$$

It can be seen that k_p is real for $-N_z \leq n \leq N_z$, otherwise, k_p is imaginary. Therefore, only those modes in the visible region are propagation modes. They can propagate to far region and contribute to the far-field. The other modes are all evanescent modes because their amplitudes decay exponentially when they travel away from the z-axis and do not contribute to the far-field.

Therefore, the far-field of the linear source can be rigorously expressed as

$$F_a(\theta) = \sum_{n=-N_x}^{N_x} I_n f_n(\theta) \quad (8)$$

As can be seen clearly from (8), the far-field of the linear source is simply the superposition of the sinc mode functions. As the mode functions are independent to each other, (8) proves that the degree of freedom (DoF) of the far field of the linear source with length of $N_x \lambda$ is exactly $2N_x + 1$, which has been demonstrated by Miller in [32], and is approximately in agreement with the result proposed in [33]. For a linear current with length of 4λ , there are 9 propagation modes. The mode functions are shown in Fig.2, and the corresponding beam at the center and at the bottom are shown in Fig.3.

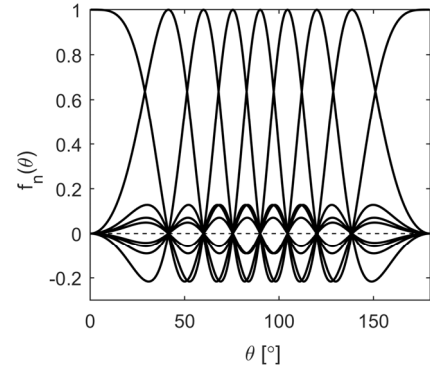


Fig.2 The 9 mode functions for the linear current with length of 4λ .

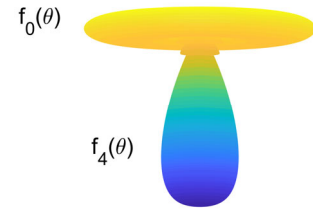


Fig.3 The beams associated with $f_0(\theta)$ and $f_4(\theta)$.

It is very important to note from the property of the sinc function that, under condition of $D_z = N_z \lambda$, we have $f_n(\theta_n) = 1$, and $f_n(\theta_m) = 0$ for $m \neq n$. Therefore, (8) is the ideal interpolation of the far-field using the sinc mode functions and I_n are simply the interpolation values of the far-field at the sampling points ($\theta = \theta_n$). Consequently, the coefficient of the Fourier series of the current can be directly picked out as $I_n = F_a(\theta_n)$, so the current source to realize the prescribed far-field pattern is obtained immediately,

$$I(z) = \sum_{n=-N_x}^{N_x} I_n e^{jn\Omega z} = \sum_{n=-N_x}^{N_x} F_a(\theta_n) e^{jn\Omega z} \quad (9)$$

with θ_n is given in (7). The synthesis is completed without necessity of involving any optimization. For very large array, (9) can be evaluated efficiently with FFT.

Three examples are used to validate the synthesis method. The first two arrays, Array-1 and Array-2, both have a single main lobe. Their far-field pattern prototypes are shown in Fig. 4.

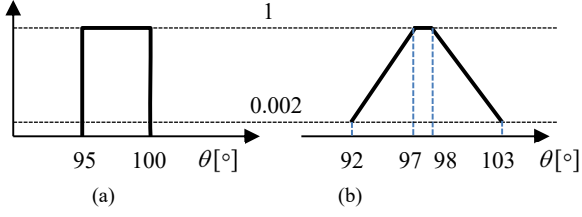


Fig.4 Prototype of the far-field pattern. (a) Array-1. (b) Array-2.

Assume to realize the far-field patterns using a linear current with length of 100λ . There are total 201 mode functions, the peak position of each mode function can be calculated with (7). For Array-1, the current coefficient can be determined with

$$I_n = \begin{cases} 1, & 95^\circ \leq \theta_n \leq 100^\circ \\ 0, & \text{otherwise} \end{cases}$$

The realized far-field pattern is calculated with (8), as shown in Fig.5(a).

A transition region of 5 degree is assigned in Array-2. The sidelobe level is restricted to 0.002, or -54dB. The realized far-field pattern is shown in Fig.5(b). As is expected, the sidelobe level can be greatly reduced for arrays with smooth transition bands.

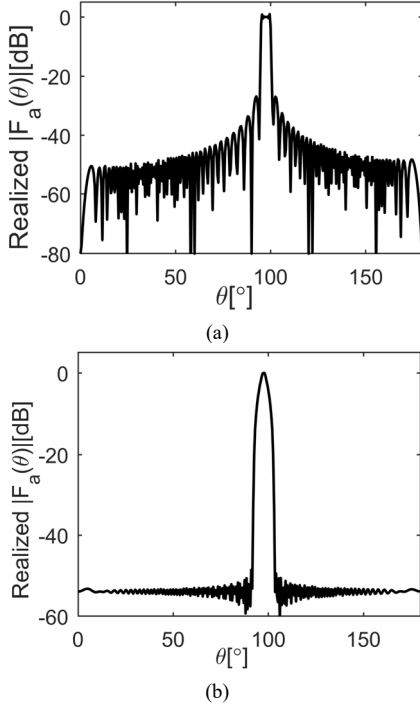


Fig.5 Realized far-field pattern. (a) Array-1. (b) Array-2.

The linear current used to realize these patterns are calculated with (9). Their amplitudes are plotted in Fig.6.

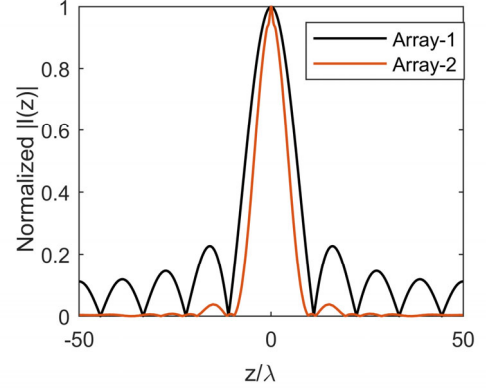


Fig.6 The synthesized current distributions for the two arrays.

The third example (Array-3) has two beams, with its far-field prototype shown in Fig.7(a). It has a 2° transition region at each edge. It is realized with a linear source with length of 1000λ . The realized far-field pattern is shown in Fig.7(b). Although it is not plotted here, the current needed for realizing this radiation pattern can be obtained in the same manner.

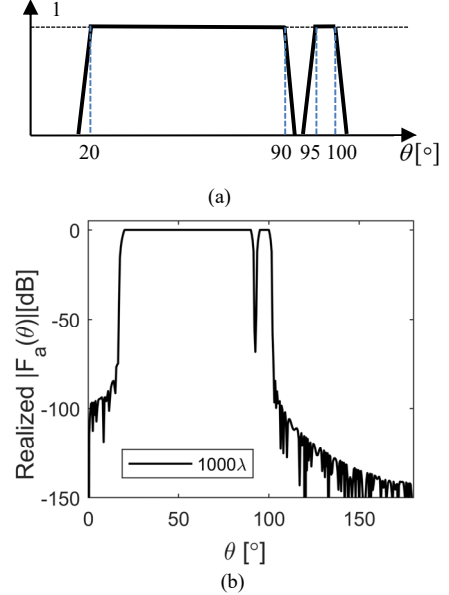


Fig.7 Array-3. (a) Prototype. (b) The realized far-field pattern.

III. TWO-DIMENSIONAL CASE

Consider a current source on a rectangular sheet in the xoy plane, centering at the origin. The far field of the current can be expressed from (1) as

$$\mathbf{F}(\theta, \varphi) = -\sin \theta_x \hat{\theta}_x \int_{-D_y/2}^{D_y/2} \int_{-D_x/2}^{D_x/2} e^{jk_x x + jk_y y} I_x(x, y) dx dy - \sin \theta_y \hat{\theta}_y \int_{-D_y/2}^{D_y/2} \int_{-D_x/2}^{D_x/2} e^{jk_x x + jk_y y} I_y(x, y) dx dy \quad (10)$$

where θ_x is the angle between the position vector \mathbf{r} and the x -axis, and θ_y is that with the y -axis. $\hat{\theta}_x$ and $\hat{\theta}_y$ are respectively the corresponding unit vectors, as shown in Fig. 8.

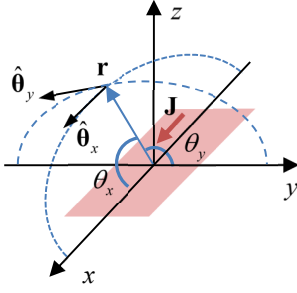


Fig.8 Current sheet and the unit vectors in the coordinate system.

Similar to that in the 1-D case, the factor $\sin \theta_x$ and $\sin \theta_y$ come from the x -polarized infinitesimal dipole and the y -polarized infinitesimal dipole composing the current sheet. (10) shows that the x -component and the y -component of the current can be handled separately because their far fields are separable at every direction,

$$\mathbf{F}(\theta, \varphi) \cdot \hat{\theta}_x = -\sin \theta_x \int_{-D_y/2}^{D_y/2} \int_{-D_x/2}^{D_x/2} e^{jk_x x + jk_y y} I_x(x, y) dx dy \quad (11)$$

$$\mathbf{F}(\theta, \varphi) \cdot \hat{\theta}_y = -\sin \theta_y \int_{-D_y/2}^{D_y/2} \int_{-D_x/2}^{D_x/2} e^{jk_x x + jk_y y} I_y(x, y) dx dy \quad (12)$$

Take the x -polarization as an example. We consider the 2-D array factor,

$$F_{2ax}(\theta, \varphi) = \frac{1}{D_x D_y} \int_{-D_y/2}^{D_y/2} \int_{-D_x/2}^{D_x/2} e^{jk_x x + jk_y y} I_x(x, y) dx dy \quad (13)$$

Here again we have added a constant factor $1/(D_x D_y)$ for the sake of convenience. The planar current is now expanded as a 2-D Fourier series,

$$I_x(x, y) = \sum_{m=-\infty}^{\infty} \sum_{n=-\infty}^{\infty} I_{xmn} e^{j(m\Omega_x x + n\Omega_y y)} \quad (14)$$

where $\Omega_x = 2\pi/D_x$ and $\Omega_y = 2\pi/D_y$. In this paper, we choose $D_x = N_x \lambda$ and $D_y = N_y \lambda$. Substituting (14) into (13) gives

$$F_{2ax}(\theta, \varphi) = \sum_{m=-\infty}^{\infty} \sum_{n=-\infty}^{\infty} I_{xmn} f_{xmn}(\theta, \varphi) \quad (15)$$

The 2-D mode function $f_{xmn}(\theta, \varphi)$ for the x -polarization is expressed by

$$f_{xmn}(\theta, \varphi) = \text{sinc} \left[\frac{D_x}{2} (k \sin \theta \cos \varphi + m\Omega_x) \right] \times \text{sinc} \left[\frac{D_y}{2} (k \sin \theta \sin \varphi + n\Omega_y) \right] \quad (16)$$

which describes a beam in the space with its peak at the direction of $(\theta_{mn}, \varphi_{mn})$ satisfying

$$\begin{cases} k \sin \theta_{mn} \cos \varphi_{mn} + m\Omega_x = 0 \\ k \sin \theta_{mn} \sin \varphi_{mn} + n\Omega_y = 0 \end{cases} \quad (17)$$

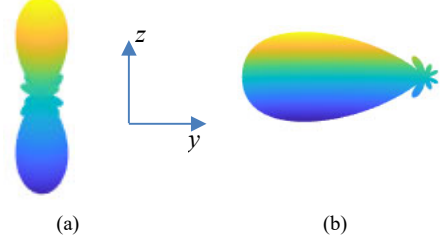
In the visible region, $0 \leq \theta_{mn} \leq \pi$ and $0 \leq \varphi_{mn} \leq 2\pi$, it can be derived from (17) that

$$(m\Omega_x)^2 + (n\Omega_y)^2 = k^2 \sin^2 \theta_{mn} \leq k^2$$

which leads to

$$(m/N_x)^2 + (n/N_y)^2 \leq 1 \quad (18)$$

Notice that $(\pi - \theta_{mn}, \varphi_{mn})$ also satisfy (17). Therefore, each 2-D mode function in the visible region is associated with a beam having two main lobes symmetrically located in the two sides of the source plane. For a $2\lambda \times 2\lambda$ current sheet, the two beams associated with $f_{00}(\theta, \varphi)$ and $f_{02}(\theta, \varphi)$ are shown in Fig. 9.

Fig.9 The beams associated with the 2-D mode function, (a) $f_{00}(\theta, \varphi)$, and (b) $f_{02}(\theta, \varphi)$.

In 2-D case, we have $k_x = k \sin \theta \cos \varphi$, $k_y = k \sin \theta \sin \varphi$, and $k_z = k \cos \theta$. Therefore, the wavenumber of the mn -th mode can be found from (17) as

$$\begin{cases} k_{xmn} = k \sin \theta_{mn} \cos \varphi_{mn} = -m\Omega_x = -km/N_x \\ k_{ymn} = k \sin \theta_{mn} \sin \varphi_{mn} = -n\Omega_y = -kn/N_y \end{cases}$$

and

$$k_{zmn} = \pm k \sqrt{1 - (m/N_x)^2 - (n/N_y)^2} \quad (19)$$

For the sake of convenience, we define a set \mathbb{P} of integer pairs as

$$\mathbb{P} = \left\{ (m, n) \in \mathbb{Z}^2 : (m/N_x)^2 + (n/N_y)^2 \leq 1 \right\}$$

Like in the 1-D case, we can check that if $(m, n) \in \mathbb{P}$, then k_{zmn} is real. The corresponding mode is a propagation mode in $\pm z$ direction. It can leave the source plane and contribute to the far-field of the source. Otherwise, the mode is an evanescent one and decays exponentially with $|z|$. It has no contribution to the far-field pattern. Therefore, the far-field of the x -component of the current sheet can be exactly expressed by

$$F_{2ax}(\theta, \varphi) = \sum_{m=-N_x}^{N_x} \sum_{n=-N_y}^{N_y} I_{xmn} f_{xmn}(\theta, \varphi), \quad (m, n) \in \mathbb{P} \quad (20)$$

The DoF of the far-field can be strictly counted using (18). Generally speaking, one rectangular current sheet has two perpendicular components. The total degree of freedom should be twice of that of the single polarization current.

Under the condition that $D_x = N_x \lambda$ and $D_y = N_y \lambda$, we can check that $f_{xmn}(\theta_{mn}, \varphi_{mn}) = 1$, and $f_{xmn}(\theta_{pq}, \varphi_{pq}) = 0$ if $p \neq m$, or $q \neq n$. Therefore, (20) is the ideal interpolation of the far-field of the 2-D source with the 2-D mode functions, and I_{xmn} is the sampling values of the far-field at the peak direction of $(\theta_{mn}, \varphi_{mn})$. We can obtain the coefficients of the current sheet directly as $I_{xmn} = F_{2ax}(\theta_{mn}, \varphi_{mn})$. The x -component of the current distribution for realizing the prescribed x -polarized far-field pattern $F_{2ax}(\theta, \varphi)$ can be explicitly expressed as

$$I_x(x, y) = \sum_{m=-N_x}^{N_x} \sum_{n=-N_y}^{N_y} F_{2ax}(\theta_{mn}, \varphi_{mn}) e^{j(m\Omega_x x + n\Omega_y y)} \quad (21)$$

with $(m, n) \in \mathbb{P}$.

As an example, we are now to realize a far-field pattern with the shape of two letters “6G”. The source area is chosen to be $60\lambda \times 60\lambda$. We can directly synthesize the current distribution with the following steps,

Step 1: Define the area for “6G” in the $k_x - k_y$ plane where k_z is real, which is the blue area in Fig.10.

Step 2: Use (17) and (18) to select the mode whose peak direction $(\theta_{mn}, \varphi_{mn})$ falls in the “6G” area.

Step 3: Use these selected modes to synthesize the current distribution with (21), and the realized far-field pattern with (20).

All these steps can be carried out very fast with MatLab codes in a notebook computer. There are total 11289 propagation modes. Among them, 1504 modes are used to realize the “6G” pattern.

The realized far-field pattern is shown in Fig.11. Since it is symmetrical with respect to source plane, only the upper half part of the radiation pattern is plotted. The amplitude of the current distribution is shown in Fig.12. Apparently, the current is concentrated in the center area may have very small amplitude in most of the other areas.

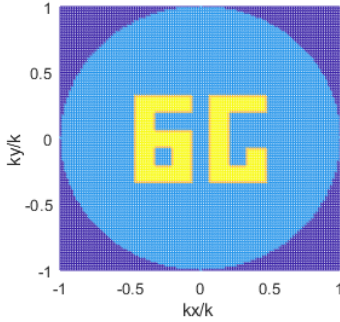


Fig.10 Defining the area for the pattern “6G” in the $k_x - k_y$ plane.

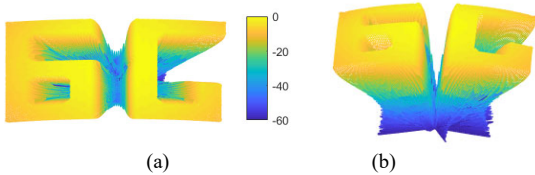


Fig.11 Realized far-field pattern. (a) Top view. (b) Front side view.

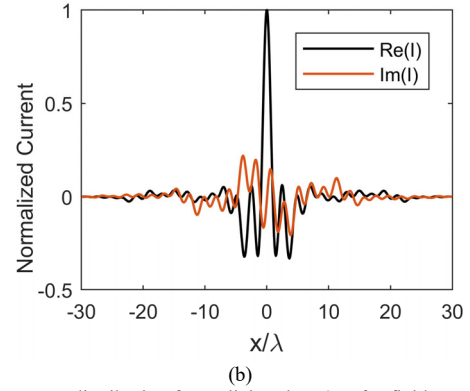
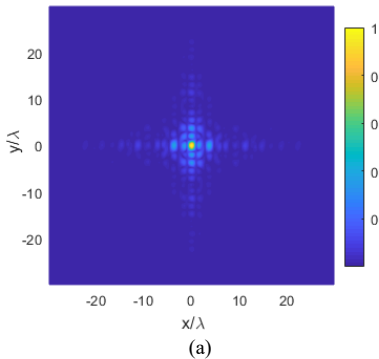


Fig.12 Current distribution for realizing the “6G” far-field pattern. (a) Top view. (b) Along the x-axis.

IV. DISCUSSIONS AND CONCLUSIONS

The key skills adopted in this direct synthesis method are summarized as follows:

(1) By setting the size of a linear current or a rectangular current sheet to be multiple wavelengths in one dimension, the mode functions are all sinc functions. Their zeros are all overlapped, and at the peak of one mode function, all other mode functions are zero.

(2) By checking the behavior in the direction perpendicular to the sources, the beams associated with the mode functions are separated into propagation modes and evanescent modes. The far-field only include the contributions from the propagation modes in the visible region.

(3) Using the sinc mode functions, the far-field of the source is exactly expressed as an interpolation of the sampling values at the peak directions of the propagation beams. The coefficient of the Fourier series of the current can be directly obtained owing to the special property of the sinc functions.

It is also very important to emphasize one fact here: the current expressed in (9) and (21) are all band limited in k -space, or we may describe them as spatially band limited because the wavenumber can actually be treated as spatial frequency in electromagnetic theory. They are the currents required to realize the prescribed far-field pattern. In free space, these currents completely determine the far-field pattern. However, a practical current is not necessary to be band-limited in k -space. The currents are generally expressed with (4) or (14) instead of (9) or (21). Take the 2-D case as an example. We can see this issue more clearly by dividing the general current source expressed in (14) into two parts,

$$I_x(x, y) = I_x^{rad}(x, y) + I_x^{eva}(x, y) \quad (22)$$

where

$$I_x^{rad}(x, y) = \sum_m \sum_n I_{xmn} e^{j(m\Omega_x x + n\Omega_y y)}, (m, n) \in \mathbb{P} \quad (23)$$

$$I_x^{eva}(x, y) = \sum_m \sum_n I_{xmn} e^{j(m\Omega_x x + n\Omega_y y)}, (m, n) \notin \mathbb{P} \quad (24)$$

As has been demonstrated in previous section that the far-field is completely determined by $I_x^{rad}(x, y)$ and is not affected by $I_x^{eva}(x, y)$. $I_x^{eva}(x, y)$ creates only evanescent modes in the space. However, it causes energy storage surrounding the source and may affect the property at the excitation ports for a real array. Therefore, it is possible to adjust the current

$I_x^{eva}(x, y)$ in a real array so that it can be excited more easily, while in the meantime keep the radiative pattern unchanged if we can keep $I_x^{rad}(x, y)$ unchanged. This is why similar radiation patterns can be realized with quite different current distributions in many practical arrays. The conventional optimization algorithm can still play a powerful role in finding a proper solution when external factors, such as the excitation conditions, are taken into account.

In practical applications, it may be difficult to realize a continuous array factor. We may need to spatially sample the continuous current associated with the array factor and realize the far-field pattern using discrete elements with a half wavelength spacing. This discretization corresponds to spatial sampling frequency of $2\pi/(0.5\lambda) = 2k$ in k -space, which is 2 times higher than largest spatial frequency k of the propagation modes. Therefore, if the current of the array factor is band-limited expressed by (21), by sampling the continuous array factor with spacing of smaller than or equal to half wavelength, the resultant higher harmonic components in the current only brings evanescent modes. They basically do not affect the far-field pattern of the antenna array. However, if the current is not spatially band-limited, then, discretization may affect the radiation pattern because of aliasing effect.

With the method proposed here, the current for realizing a far-field pattern is directly synthesized. Positively, it is the exact way to realize the pattern if we can practically create the resultant spatially band-limited current distribution. At least it can provide us a reference for realizing the pattern with equally-spaced or nonequally-spaced discrete elements. It is also a good reference for further thinning the array because we can simply drop those currents with amplitude smaller than a given criterion.

REFERENCES

- [1] F. Rusek et al., "Scaling up MIMO: opportunities and challenges with very large arrays," *IEEE Sig. Process. Mag.*, vol. 30, no. 1, pp. 40-60, Jan. 2013.
- [2] E. G. Larsson, O. Edfors, F. Tufvesson, and T. L. Marzetta, "Massive MIMO for next generation wireless systems," *IEEE Commun. Mag.*, vol. 52, no. 2, pp. 186-195, Feb. 2014.
- [3] P. J. Napier, A. R. Thompson and R. D. Ekers, "The very large array: Design and performance of a modern synthesis radio telescope," *Proc. IEEE*, vol. 71, no. 11, pp. 1295-1320, Nov. 1983.
- [4] S. Pan, X. Ye, Y. Zhang and F. Zhang, "Microwave Photonic Array Radars," *IEEE J. Microwaves*, vol. 1, no. 1, pp. 176-190, Jan. 2021.
- [5] F. Ares, R. S. Elliott and E. Moreno, "Design of planar arrays to obtain efficient footprint patterns with an arbitrary footprint boundary," *IEEE Trans. Antennas Propag.*, vol. 42, no. 11, pp. 1509-1514, Nov. 1994.
- [6] O. M. Bucci, G. D'Elia, G. Mazzarella and G. Panariello, "Antenna pattern synthesis: a new general approach," *Proc. IEEE*, vol. 82, no. 3, pp. 358-371, Mar. 1994.
- [7] J. A. Rodriguez, F. Ares, P. Lopez and E. Moreno, "Quasi-analytical synthesis of moderate and large arrays radiating arbitrary 'Star-Shaped' footprint patterns [Antenna Designer's Notebook]," *IEEE Antennas Propag. Mag.*, vol. 49, no. 5, pp. 105-112, Oct. 2007.
- [8] F. Ares, J. Fondevila-Gomez, G. Franceschetti, E. Moreno-Piquero and J. A. Rodriguez-Gonzalez, "Synthesis of very large planar arrays for prescribed footprint illumination," *IEEE Trans. Antennas Propag.*, vol. 56, no. 2, pp. 584-589, Feb. 2008.
- [9] A. Aghasi, H. Amindavar, E. L. Miller and J. Rashed-Mohassel, "Flat-top footprint pattern synthesis through the design of arbitrary planar-shaped apertures," *IEEE Trans. Antennas Propag.*, vol. 58, no. 8, pp. 2539-2552, Aug. 2010.
- [10] W. P. M. N. Keizer, "Fast low-sidelobe synthesis for large planar array antennas utilizing successive Fast Fourier Transforms of the array factor," *IEEE Trans. Antennas Propag.*, vol. 55, no. 3, pp. 715-722, Mar. 2007.
- [11] S. Caorsi, A. Lommi, A. Massa, and M. Pastorino, "Peak sidelobe reduction with a hybrid approach based on GAs and difference sets," *IEEE Trans. Antennas Propag.*, vol. 52, no. 4, pp. 1116-1121, Apr. 2004.
- [12] K. Yang, Z. Zhao, Q. H. Liu, "Fast pencil beam pattern synthesis of large unequally spaced antenna arrays," *IEEE Trans. Antennas Propag.*, vol. 61, no. 2, pp. 627-634, Feb. 2013.
- [13] W. Hong et al., "Multibeam antenna technologies for 5g wireless communications," *IEEE Trans. Antennas Propag.*, vol. 65, no. 12, pp. 6231-6249, Dec. 2017.
- [14] R. L. Haupt, "Thinned arrays using genetic algorithms," *IEEE Trans. Antennas Propag.*, vol. 42, no. 7, pp. 993-999, Jul. 1994.
- [15] J. M. Johnson and V. Rahmat-Samii, "Genetic algorithms in engineering electromagnetics," *IEEE Antennas Propag. Mag.*, vol. 39, no. 4, pp. 7-21, Aug. 1997.
- [16] D. Boeringer and D. Werner, "Particle swarm optimization versus genetic algorithms for phased array synthesis," *IEEE Trans. Antennas Propag.*, vol. 52, no. 3, pp. 771-779, Mar. 2004.
- [17] C. A. Meijer, "Simulated annealing in the design of thinned arrays having low sidelobe levels," *Proc. South African Symp. Comm. Signal Processing*, pp. 361-366, 1998.
- [18] B. Fuchs, "Synthesis of sparse arrays with focused or shaped beam pattern via sequential convex optimizations," *IEEE Trans. Antennas Propag.*, vol. 60, no. 7, pp. 3499-3503, Jul. 2012.
- [19] G. Prisco and M. D'Urso, "Maximally sparse arrays via sequential convex optimizations," *IEEE Antennas Wireless Propag. Lett.*, vol. 11, pp. 192-195, 2012.
- [20] O. Quevedo-Teruel and E. Rajo-Iglesias, "Ant colony optimization in thinned array synthesis with minimum sidelobe level," *IEEE Antennas Wirel. Propag. Lett.*, vol. 5, pp. 349-352, 2006.
- [21] T. G. Spence and D. H. Werner, "Design of broadband planar arrays based on the optimization of aperiodic dilutions," *IEEE Trans. Antennas Propag.*, vol. 56, no. 1, pp. 76-86, Jan. 2008.
- [22] R. L. Haupt, "Interleaved thinned linear arrays," *IEEE Trans. Antennas Propag.*, vol. 53, no. 9, pp. 2858-2864, Sept. 2005.
- [23] K. Chellapilla and A. Hoorfar, "Evolutionary programming: an efficient alternative to genetic algorithms for electromagnetic optimization problems," *IEEE Antennas Propag. Society Int. Symp. 1998 Digest*, pp. 42-45 vol.1, 1998.
- [24] D. Leeper, "Isophoric arrays-massively thinned phased arrays with well controlled sidelobes," *IEEE Trans. Antennas Propag.*, vol. 47, no. 12, pp. 1825-1835, Dec. 1999.
- [25] G. Oliveri, M. Donelli, and A. Massa, "Linear array thinning exploiting almost difference sets," *IEEE Trans. Antennas Propag.*, vol. 57, no. 12, pp. 3800-3812, Dec. 2009.
- [26] N. Anselmi, G. Gottardi, G. Oliveri and A. Massa, "A total-variation sparseness-promoting method for the synthesis of contiguously clustered linear arrays," *IEEE Trans. Antennas Propag.*, vol. 67, no. 7, pp. 4589-4601, July 2019.
- [27] G. Oliveri, L. Manica, and A. Massa, "ADS-based guidelines for thinned planar arrays," *IEEE Trans. Antennas Propag.*, vol. 58, no. 6, pp. 1935-1948, Jun. 2010.
- [28] A. Aldhafeeri and Y. Rahmat-Samii, "Brain storm optimization for electromagnetic applications: continuous and discrete," *IEEE Trans. Antennas Propag.*, vol. 67, no. 4, pp. 2710-2722, April 2019.
- [29] D. Caratelli, G. Toso, O. V. Stukach and N. V. Panokin, "Deterministic constrained synthesis technique for conformal aperiodic linear antenna arrays—Part II: applications," *IEEE Trans. Antennas Propag.*, vol. 67, no. 9, pp. 5962-5973, Sept. 2019.
- [30] O. M. Bucci, M. D'Urso, T. Isernia, P. Angeletti, and G. Toso, "Deterministic synthesis of uniform amplitude sparse arrays via new density taper techniques," *IEEE Trans. Antennas Propag.*, vol. 58, no. 6, pp. 1949-1958, Feb. 2010.
- [31] B. P. Kumar and G. R. Branner, "Generalized analytical technique for the synthesis of unequally spaced arrays with linear, planar, cylindrical or spherical geometry," *IEEE Trans. Antennas Propag.*, vol. 53, no. 2, pp. 621-633, Feb. 2005.
- [32] E. K. Miller, "The incremental far field and degrees of freedom of the sinusoidal current filament," *IEEE Antennas Propag. Mag.*, vol. 49, no. 4, pp. 13-21, Aug. 2007.
- [33] A. Pizzo, T. L. Marzetta and L. Sanguinetti, "Degrees of freedom of holographic MIMO channels," *2020 IEEE 21st Int. Workshop Sig. Proc. Advances Wirel. Comm. (SPAWC)*, pp. 1-5, 2020.